ELSEVIER

S0032-3861(96)00168-1

Polymer Vol. 37 No. 16, pp. 3593–3601, 1996

0032-3861/96/$15.00+0.00

Diffusion phenomena during cyanate resin cure

Yong Deng and George C. Martin*
Department of Chemical Engineering and Materials Science, Syracuse University, Syracuse, NY 13244, USA
(Received 4 May 1995; revised 24 July 1995)

The diffusion phenomena, including the molecular diffusion processes and the effect of diffusion on the cure kinetics and molecular size distribution, during the curing of a zinc-catalysed cyanate ester resin have been studied. The average diffusivity, which was estimated using the dielectric analysis-based approach, decreased by several orders of magnitude during the curing process. The molecular size distribution measured with size exclusion chromatography was found to deviate from the mean-field prediction at relatively high conversions. By using the Rabinowitch model, a diffusion-controlled kinetic model was formulated, which adequately predicted the experimental cyanate conversion profiles over the entire range of cure. Copyright © 1996 Elsevier Science Ltd.

(Keywords: cyanate ester resins; diffusion; diffusion-controlled kinetics)

INTRODUCTION

Cyanate ester resins represent one class of thermosetting, high-performance materials that are being evaluated for structural and electronic applications. Their attractive features include low dielectric loss factors, high glass transition temperatures (T_gs), excellent adhesion characteristics, low water adsorption, good mechanical properties, monomer purity, dimensional stability at solder temperatures, and ease of processing.

The curing of cyanate resins has been the main subject of a number of recent publications[1–6]. The major reaction pathway is the cyclotrimerization of cyanate groups to form triazines[7–10]. Cyanates also react with various hydroxyl groups to form imidocarbonates[7,8,11]; the presence of hydroxyl groups may be due to phenols in the form of impurities or catalysts, or any adventitious water in the system. During commercial processing of cyanate resins, coordination metals are usually used as catalysts and phenols as co-catalysts. In the presence of a metal catalyst, the overall reaction obeys a second-order rate law with respect to cyanate concentration while, in the absence of metal catalysts, the reaction is autocatalytic[1,2,9]. It has been found that the reaction kinetics of both the uncatalysed and the metal-catalysed systems may also be adequately described by a unified model, a second-order and a second-order autocatalytic model[4].

While the curing of many epoxy resins, such as epoxy-amines, is significantly influenced by the molecular diffusion processes mainly in the post-vitrification stage, the reaction of cyanate resins has been found to become diffusion-controlled even in the pre-gel stage[3,4,9]. Since, under diffusional limitations, the diffusivities and reactivities of the molecular species are functions of their sizes, the network formation process is expected to be cure path-dependent. Therefore, the diffusion control may affect not only the reaction kinetics but also the structure–property relationship. In order to optimize the curing processes for the cyanate resins, it is very important to understand the diffusion-related phenomena.

Recently, a modelling strategy has been developed for characterizing the diffusion processes during cure[12,13]. This approach is based on the dynamic dielectric analysis of the curing system and is composed mainly of two relations:

$$D = \frac{K_2}{K_1}\sigma \bar{x}_n^{-1} \quad (1)$$

$$D\tau^n = K_3 \quad (2)$$

where D is the average diffusion coefficient of the monomer units, σ is the ionic conductivity, $\bar{x}_n$ is the number-average degree of polymerization, τ is the dipole relaxation time, n is the power-law index independent of cure and temperature, and K_1, K_2, and K_3 are constants at isothermal conditions.

In a curing system, there are always certain ionic species in addition to the molecular species. The ionic species may be due to impurities or catalysts in the system. Equation (1) was derived by considering the ionic species as probes to the molecular diffusion processes. This equation may be used to estimate the overall diffusion in the pre-gel stage and the sol diffusion in the post-gel stage. Equation (2) was obtained from the free-volume theory and is valid over the entire range of cure. One way to evaluate the power-law index n is to use equation (2) by measuring the relaxation times of pre-gel samples and determining the corresponding diffusion

* To whom correspondence should be addressed

coefficients using equation (1). The average diffusion coefficient in the post-gel stage may then be found by measuring the dipole relaxation time of the resin.

The overall diffusion coefficient in the post-gel stage may also be evaluated based on the sol diffusion coefficient alone, if, over the range of cure of interest, the sol fraction or weight fraction of solubles is not much smaller than the gel fraction[12,13]

$$D \approx w_s D_s = \frac{K_2}{K_1} \sigma \bar{x}_{ns}^{-1} w_s \tag{3}$$

where w_s is the sol fraction, D_s is the diffusion coefficient of solubles, and $\bar{x}_{ns}$ is the number-average degree of polymerization of the solubles. This equation is especially useful if dipole relaxation data are not available.

The objective of the present work was to analyse the diffusion-related phenomena during the curing of cyanate ester resins and to develop a quantitative model for predicting the diffusion-controlled cure kinetics. The resin system studied was bisphenol A dicyanate (BADCy) catalysed by 100 ppm zinc (co-catalysts were not used). The dielectric behaviour and the molecular size distribution of the resin were examined in order to estimate the molecular diffusion coefficient. Then, the diffusion-controlled cure kinetics were examined based on the Rabinowitch model[14].

EXPERIMENTAL

The cyanate resin, bisphenol A dicyanate (99.9% purity), was provided by HiTek Polymers (currently a subsidiary of Ciba Geigy). The zinc metal catalyst was supplied by Pfaltz and Bauer in the form of zinc naphthenate in mineral spirits. In preparing the resin mixture, both the dicyanate and 100 ppm catalyst (ppm metal per monomer weight) were dissolved in methylene chloride, followed by solvent flashing in a vacuum oven for approximately 4 h. The dry, crystalline sample was then stored at −21°C.

Dynamic dielectric analysis was conducted using a Micromet Eumetric System II microdielectrometer. In each experiment, a low conductivity sensor was heated to the cure temperature and then approximately 15 mg of sample was placed on the sensor to cover the entire sensing area. As the cure proceeded, the sample was repeatedly scanned by the dielectrometer from high to low frequencies ranging between 10 kHz and 0.1 Hz and the dielectric permittivity and dielectric loss factor were recorded.

Size exclusion chromatography (s.e.c.) analysis was performed using a Hewlett-Packard 1050 Series HPLC instrument. Tetrahydrofuran (THF) solvent was used to carry dilute sample solutions to pass through the system at a flow rate of 0.5 ml min^{-1}. The concentration of the sample solutions was 0.1% w/v and the amount of the injection was 20 μl. Separation occurred in a 30-cm long Polymer Laboratories PLgel 5 μm MIXED-D column and the refractive index (RI) detection was carried out at 35°C with an HP 1047A RI detector. The system was calibrated using polystyrene standards in the high molecular weight range and the polymerization products (monomer, trimer, 5-mer, and 7-mer) of the cyanate resin in the low molecular weight range. No attempts were made to determine the true molecular weights of the species.

An IBM IR/32S Fourier transform infra-red spectrometer (*FT*i.r.) was used to study the cure kinetics of the resin. During each test, the sample holder was first heated to slightly above the cure temperature. Then, a small amount of sample, encased between two NaCl cells (3.2 cm in diameter), was inserted into the sample holder and, after melting, was squeezed into a thin film. The cell temperature reached 4°C below the cure temperature in less than 2 min, when the i.r. scans were initiated. To obtain each spectrum, 15 co-added interferograms of 2 cm^{-1} resolution were taken under nitrogen atmosphere. The cyanate vibrations in the form of a doublet at 2270 and 2235 cm^{-1} were monitored and the aliphatic C–H stretch at 2950 cm^{-1} was chosen as the reference peak (the same selection of the cyanate doublet and reference has previously been adopted[9]). The cyanate conversion was then calculated using:

$$\alpha = 1 - \frac{A_c(t)A_r(0)}{A_c(0)A_r(t)} \tag{4}$$

where α is the cyanate conversion, A_c is the area of the cyanate doublet, and A_r is the area of the reference peak.

Differential scanning calorimetry (d.s.c.) tests were conducted using a Mettler DSC-30 instrument to determine the T_g of the resin. Approximately 10 mg of sample was used in each test. Prior to the curing schedule, the sample was first melted at 90°C for 3 min in order to obtain a consistent baseline. Isothermal cures were interrupted at various cure times by quenching the samples to −100°C. The samples were then scanned at a heating rate of 10°C min^{-1}. The temperature corresponding to the onset of the endothermic deflection of the baseline was taken as T_g.

Extraction studies were conducted to determine the sol fraction for post-gel samples. In each test, approximately 200 mg of sample was cured isothermally for a certain period of time in a nitrogen-purged oven and quenched immediately in liquid nitrogen. The sample was then pulverized and placed in a cellulose thimble for extraction with THF. Prior to the extraction, the thimble was pre-soaked in THF and dried under vacuum. Solvent extraction was conducted for up to 2 weeks and the thimble with the remaining sample was dried and weighed. The weight fraction of solubles was determined from the difference between the initial and final weights of the sample in the thimble. The molecular weight of the solubles was analysed using s.e.c.

A Bohlin Rheometer System was used to perform dynamic mechanical analysis (d.m.a.). During the test, a sample was placed between a pair of parallel plates (2.54 cm in diameter) and filled completely the 0.159-cm gap. As the resin cured isothermally, a strain amplitude of 1% and sinusoidal oscillations of 1 Hz were applied to one of the plates. The stress and phase angle of the other plates were recorded and used to calculate the dynamic moduli.

RESULTS AND DISCUSSION

The curing of the cyanate ester resin was first examined using *FT*i.r. and d.s.c. at temperatures ranging from 130 to 170°C. The cyanate conversion profiles obtained from i.r. are shown in *Figure 1*. At each temperature, the rate of reaction decreases with time with no evidence of

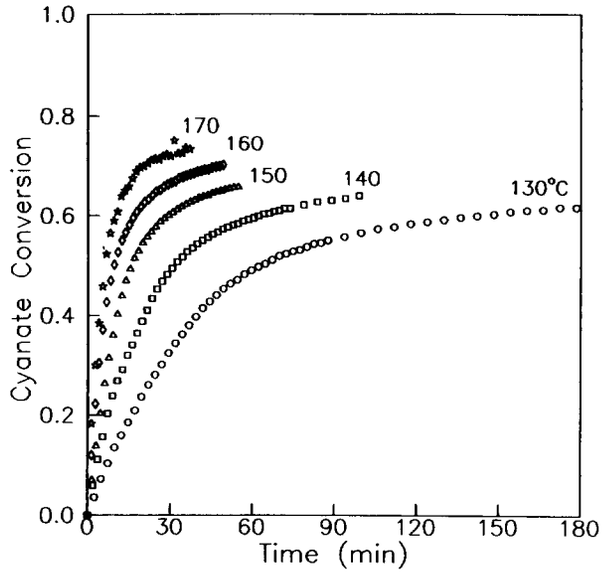

Figure 1 Cyanate conversion profiles obtained with *FT*i.r.

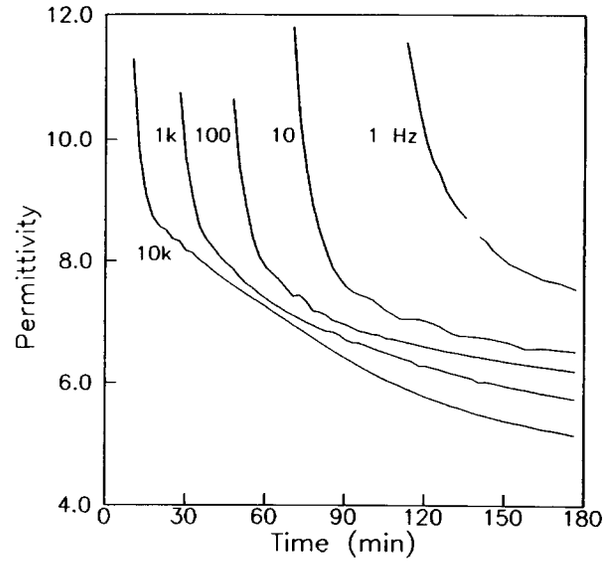

Figure 3 Dielectric permittivity at 140°C

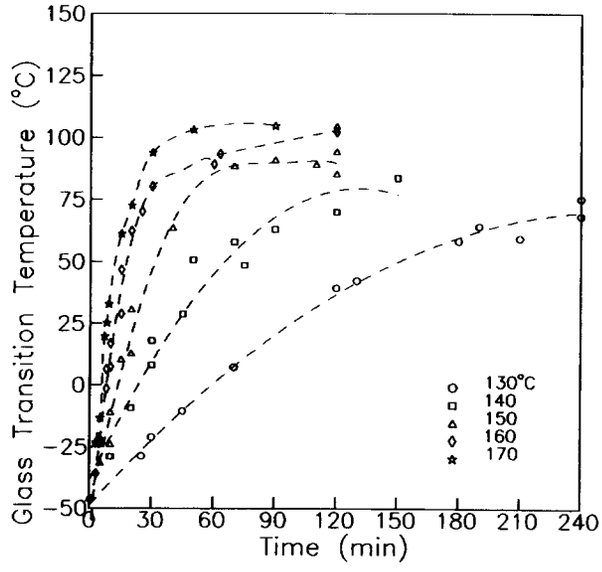

Figure 2 T_g at various cure temperatures

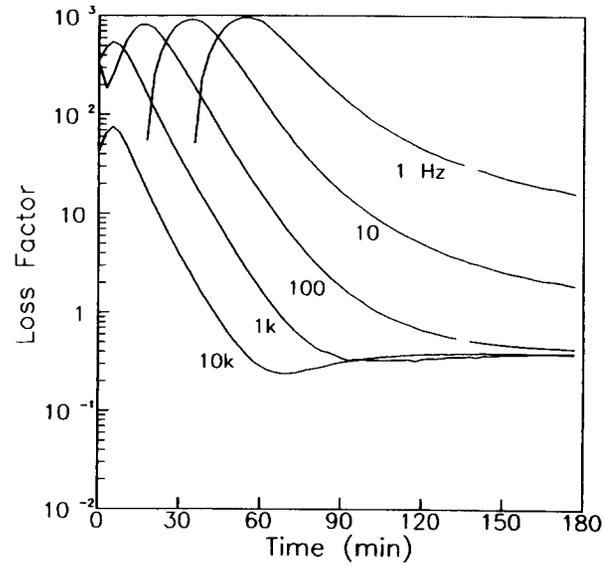

Figure 4 Dielectric loss factor at 140°C

autocatalytic effects. Thus, the autocatalytic mechanism is insignificant in the present system and the reaction is mainly catalysed by the zinc metal catalyst. As shown in *Figure 2*, the T_gs are at least 50°C lower than the cure temperatures, which means that the resin is in its rubbery state during cure.

The dielectric behaviour of the cyanate resin was analysed in order to estimate the diffusion coefficient. *Figures 3* and *4* show the dielectric permittivity and the dielectric loss factor obtained during isothermal cure at 140°C. As the resin cures, the permittivity decreases, indicating that the mobilities of ions and dipoles in the system are declining. The permittivity is very high in the early stage of cure (e.g. from 0 to 30 min at 1 kHz) and decreases rapidly. During the same period, the loss factor exhibits a peak. These phenomena may be attributed to electrode polarization induced by the applied electric field. As the cure proceeds, the loss due to ionic conduction decreases and the dipole loss becomes more significant. The high frequency loss then goes through a peak (75 min at 10 kHz) and the permittivity approaches its lower limit. Qualitatively, this is similar to what was observed for an epoxy-amine resin[15]. However, the dipole loss peaks of the cyanate resin are flat compared to those of the epoxy resin because of the absence of strong dipoles in the cyanate resin. At low frequencies (e.g. 10 and 1 Hz), the loss peaks cannot be detected.

Figures 5a and *5b* are plots of loss factor vs. permittivity for two temperatures. All the arcs formed by the dielectric data are quite flat due to the absence of strong dipoles. The resin did not reach a very high conversion at the end of each test when the reaction virtually stopped. Consequently, dielectric data over the range of low permittivities were not found. The flat and incomplete arcs of the cyanate resin make it difficult to determine dipole relaxation times even with a single frequency approach[16]. Thus, in this work, the diffusion coefficient was estimated without using either relaxation data or equation (2).

The ionic conductivity of the cyanate resin was

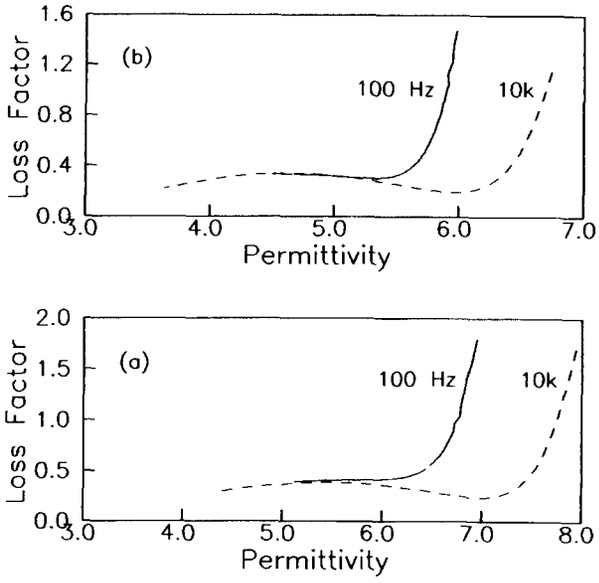

Figure 5 Loss factor vs. permittivity for the cyanate resin cured at (a) 140°C and (b) 170°C

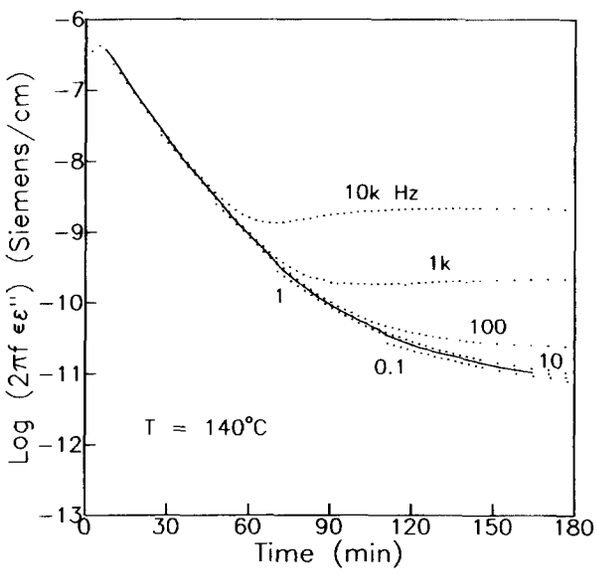

Figure 6 Extraction of ionic conductivity (solid curve) from the loss data

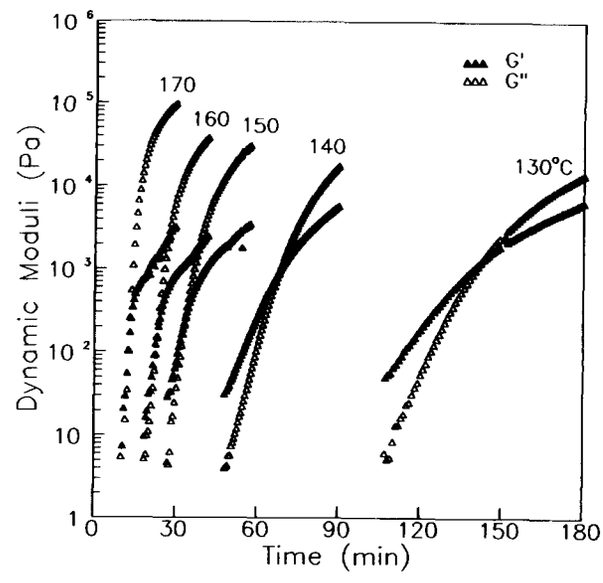

Figure 7 Storage and loss moduli at 1 Hz

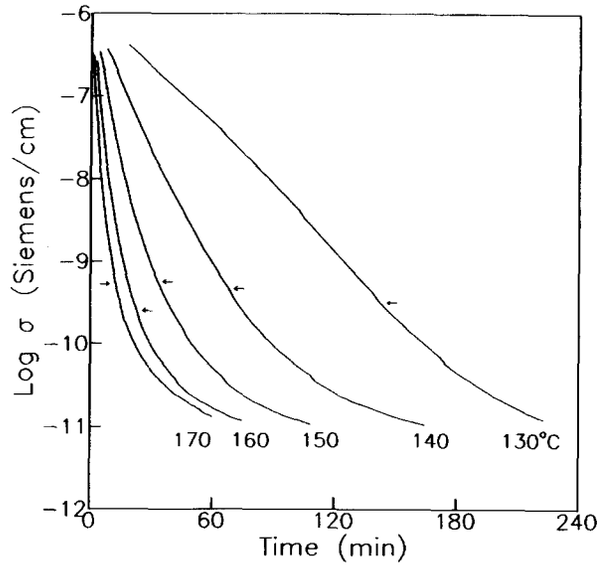

Figure 8 Ionic conductivity at various cure temperatures. The arrows indicate the gel times

extracted from the dielectric data by following a standard method[17]. In *Figure 6*, the dielectric loss factors obtained at 140°C and various frequencies were transformed into $2\pi f \in \varepsilon''$ curves (f is the frequency, ε'' is the loss factor, and $\in$ is the permittivity of free space with a value of 8.85×10^{-12} Farad m^{-1}) and were superimposed to form a single plot. Because conductivity is independent of frequency, the portion of the plot where two or more curves overlap gives the ionic conductivity. At 140°C, the electrode polarization at the onset of cure is quite intense even at the highest measurement frequency, 10 kHz, of the dielectrometer. Thus, in *Figure 6*, the conductivity data are not available at very short cure times.

Various experimental techniques have been employed for the detection of the gel point. Owusu[2] studied the gelation of BADCy catalysed by Zn, Mn, and Co catalysts with or without OH co-catalyst, and found that the gel points measured by the weight fraction of solubles, the steady shear viscosity, and the moduli crossover are in agreement. In this study, the gel point of the BADCy/100 ppm Zn system was detected by using single-frequency d.m.a. *Figure 7* shows the dynamic moduli, G' and G'', at temperatures between 130 and 170°C. Both G' and G'' increase as the cure proceeds. At the early stage of cure, G'' is larger than G', indicating a mainly viscous liquid. After gelation, G' exceeds G'' because of the elastic nature of the network formed. The G'–G'' crossover times were taken as the gel times of the system at the corresponding temperatures. Based on the gel times and the i.r. data in *Figure 1*, the gel-conversion of the resin was found to range from 60 to 64% depending on the cure temperature.

Figure 8 shows the ionic conductivity at five temperatures (the arrows indicate the gel times). The conductivity drops quickly as the cure proceeds, indicating a rapid decline in molecular mobilities.

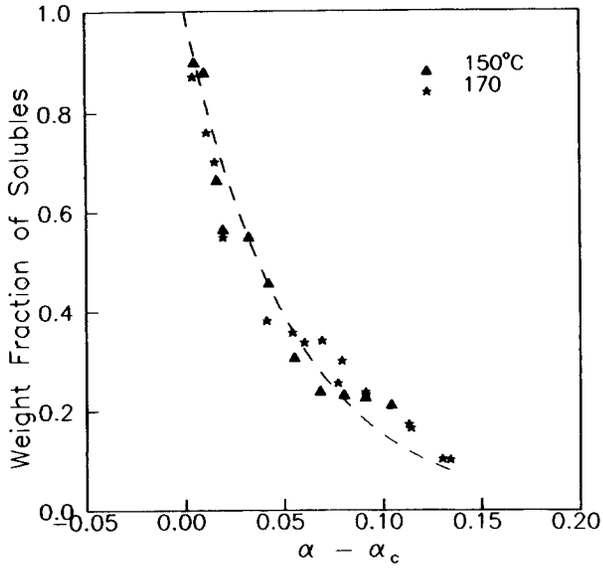

Figure 9 Weight fraction of solubles for the cyanate resin cured at 150 and 170°C. The dashed curve corresponds to equation (5)

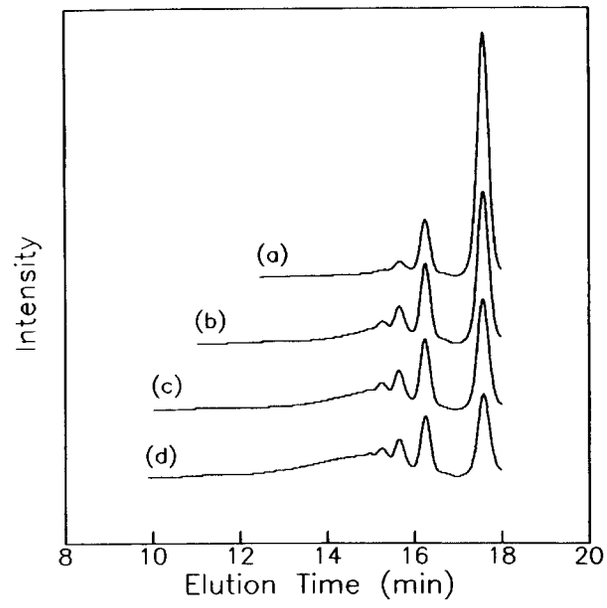

Figure 10 S.e.c. chromatograms for the pre-gel samples cured at 150°C. (a) 4 min; (b) 8 min; (c) 12 min; (d) 28 min

Extraction studies were conducted for the samples cured at 150 and 170°C in order to determine the weight fraction of solubles and the average molecular weight of the solubles. Since the gel-conversion of the cyanate resin is dependent on the cure temperature, the sol fraction is plotted in *Figure 9* against $(\alpha - \alpha_c)$, where α_c is the gel conversion. The data points at the two temperatures form overlapped curves in the figure which may be well described by the following empirical equation

$$w_s = \exp[-\kappa_1(\alpha - \alpha_c)] \tag{5}$$

where $\kappa_1 = 18.85$ for the best fit.

Note that, at the highest conversion reached by the experiments, there is still a significant amount (>10%) of solubles in the system. Thus, the gel contribution to the overall distribution is negligible and equation (3) alone may be used to determine the post-gel diffusivity[12].

S.e.c. experiments were conducted to determine the number-average degree of polymerization of the resin (the soluble portion) at various stages of cure. The pre-gel samples tested were first cured in the d.s.c. oven at isothermal conditions and the post-gel samples were obtained from the extraction studies. *Figure 10* is a plot of the chromatograms of the pre-gel samples cured at 150°C. The peaks from right to left were identified as monomer, 3-mer, and 5-mer, etc., based on the corresponding elution times and calculated molecular weights.

If cyclotrimerization of cyanates is the reaction pathway, the cyanate polymerization may be considered as a special case of A_2-B_3 copolymerization. The mean-field prediction of the molecular size distribution for the latter case has been derived by Flory[18]. For the cyanate system, the mean-field prediction is simply

$$w_i = \frac{(2i+2)!}{(i+1)!(i+2)!} p^i (1-p)^{i+2} \tag{6}$$

where w_i is the weight fraction of species with i triazines, and p is the extent of reaction.

Figures 11a–11c are plots of the normalized peak area of n-mer vs. the normalized peak area of monomer, which includes both the s.e.c. data and the weight fractions predicted by the mean-field theory. The s.e.c. data are the corresponding peak areas normalized with respect to the total area under each chromatogram. If the RI of the resin does not change during cure, the normalized peak areas are equivalent to the weight fractions of the corresponding species. The advantage in plotting the data in such a way is that the figures illustrate the original data obtained directly from the s.e.c. chromatograms – neither cure time nor conversion is used in the data reduction.

As shown in the figures, the experimental data at large monomer fractions are in agreement with the mean-field prediction. Note that, since the weight fraction of monomer decreases during cure, the data points on the right correspond to lower conversions than those on the left. The weight fraction of trimer exhibits a peak, and so does that of 5-mer, but the peaks of the s.e.c. data are located at smaller monomer fractions than those predicted by the mean-field theory. The weight fraction of $(n \geq 7)$-mers increases as the monomer fraction decreases, but at a large monomer fraction, the measured weight fraction is always smaller than the mean-field prediction. This means that when the monomer fraction is small or the conversion is relatively high, the weight fractions of short chains are larger than predicted and those of long chains are smaller than predicted. This observation indicates that, at relatively high conversions, the curing does not follow the course predicted by the mean-field theory. The three assumptions (i.e. equal reactivity, independent reactive groups, and no cycle formation) of the theory are not completely satisfied for the curing of the cyanate resin – either the cyanate groups possess unequal reactivities, or cyclization of the chains occurs, or both. Both the unequal reactivities and the cycle formation may be due to diffusion control since diffusional limitations can result in chain-length dependence of reactivities and can also restrict the movement of chains, promoting cycle formation. Note also that significant dependence of the measured weight fractions on the cure temperature is not observed.

Figure 12 illustrates the number-average molecular

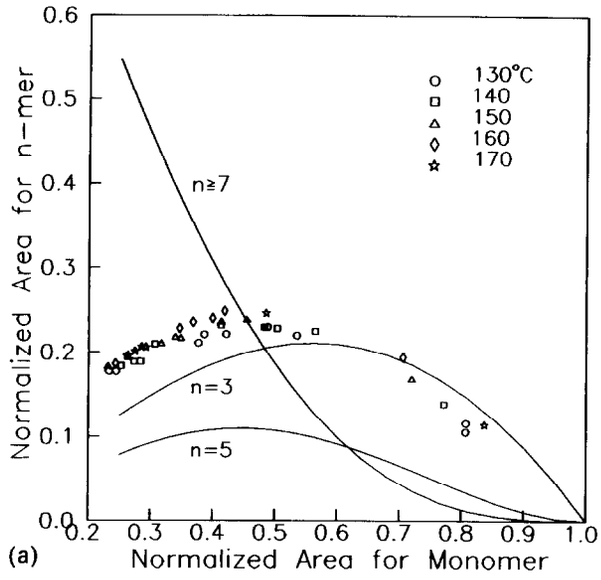

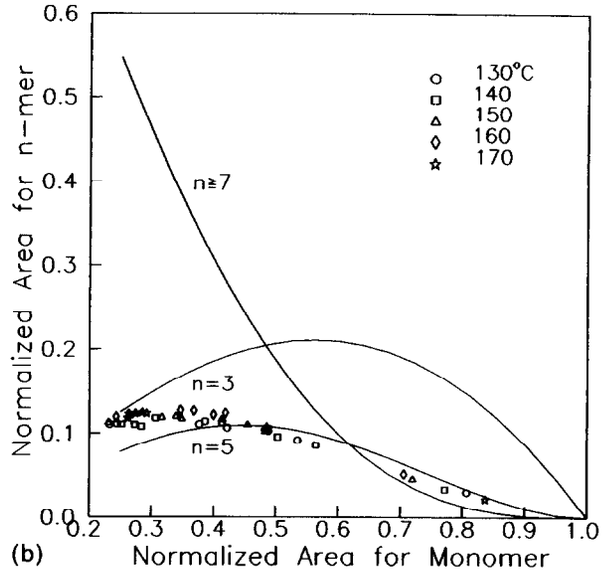

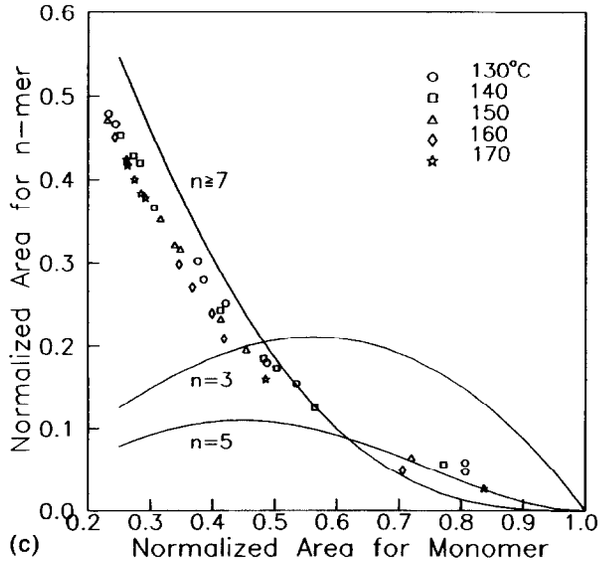

Figure 11 Comparison of the normalized s.e.c. peak area of n-mer (data points) to the weight fraction of n-mer (curve) predicted by the mean-field theory: (a) $n = 3$; (b) $n = 5$; (c) $n \geq 7$

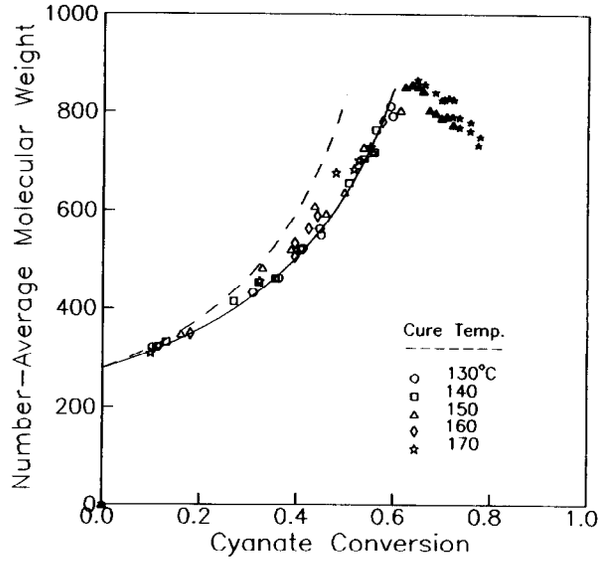

Figure 12 Number-average molecular weight vs. cyanate conversion. Data for the post-gel samples are shown with the closed symbols. The dashed curve was calculated by assuming no cycle formation and the solid curve by using equation (7)

weights evaluated based on the chromatograms; the corresponding cyanate conversions were determined using the i.r. data. The dashed curve shows the molecular weight calculated by assuming no cycle formation (see below). The average molecular weight increases with increasing conversion in the pre-gel stage and decreases in the post-gel stage. At relatively high conversions in the pre-gel stage, the number-average molecular weight is smaller than the corresponding calculated value. This discrepancy may be related to two factors. One is the cyclization of the species during cure; cycle formation always reduces the average molecular weight. The other is the use of polystyrene standards to calibrate the s.e.c., which may either increase or decrease the measured values. At the present stage, the exact effect of the standards is unknown for a cured thermoset, such as the cyanate resin, in which case the growth and branching of the chains are uncontrolled.

The experimental data show that the pre-gel average molecular weight does not exhibit cure temperature-dependence. They may be fitted to the following empirical equation (solid curve in the figure)

$$\bar{M}_n = \frac{278}{1 - \frac{4}{3}\alpha\kappa_2} \tag{7}$$

where $\kappa_2 = 0.840$ for the best fit. Note that $\kappa_2 = 1$ corresponds to the case of no cycle formation. As plotted in *Figure 13*, the post-gel molecular weight appears to be linearly dependent on $(\alpha - \alpha_c)$ over the range of conversions studied. The best linear fit is

$$\bar{M}_{ns} = \kappa_3 + \kappa_4(\alpha - \alpha_c) \tag{8}$$

where $\kappa_3 = 872$ and $\kappa_4 = 945$.

Based on the measured ionic conductivity and the above empirical relations, equations (6)–(8), the normalized diffusion coefficient was then evaluated using equations (1) and (3). Because the conductivity data are not available at the initial stage of cure, the diffusion coefficient was normalized with respect to the value at 25% conversion. *Figure 14* is a plot of the normalized

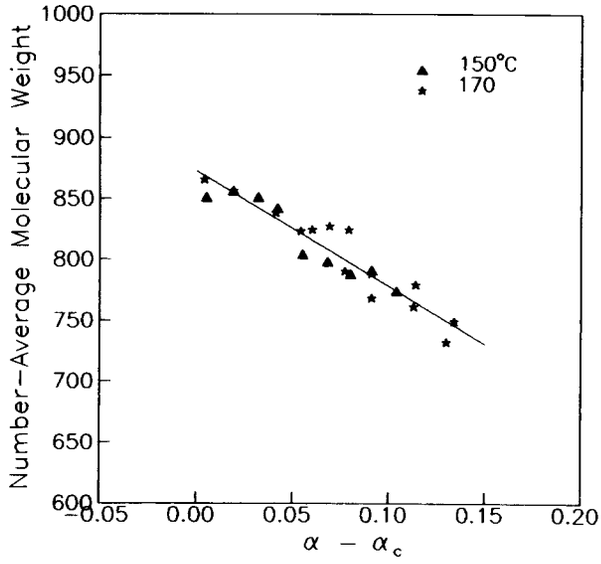

Figure 13 $\bar{M}_n$ of the solubles vs. post-gel conversion. The solid line is given by equation (8)

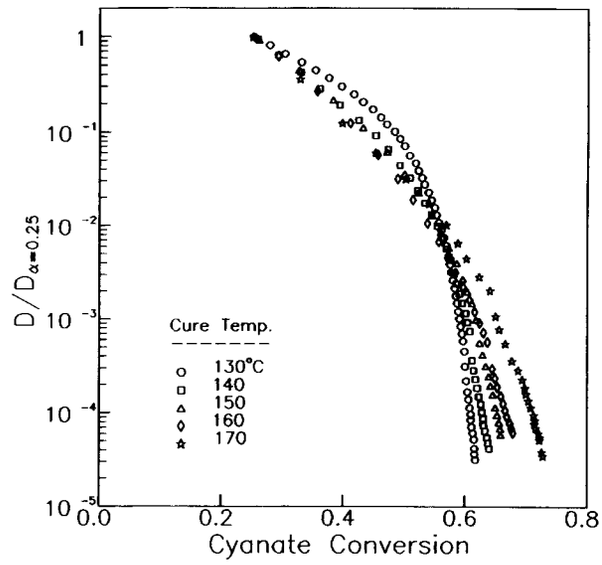

Figure 15 $D/D_{\alpha=0.25}$ vs. cyanate conversion

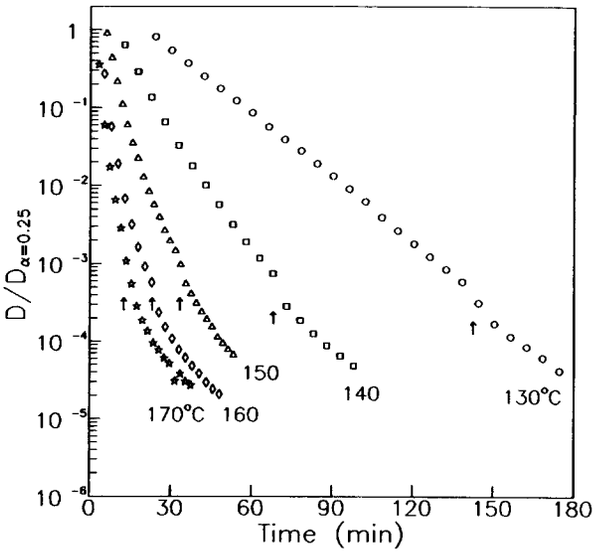

Figure 14 $D/D_{\alpha=0.25}$ vs. cure time. The arrows indicate the gel times

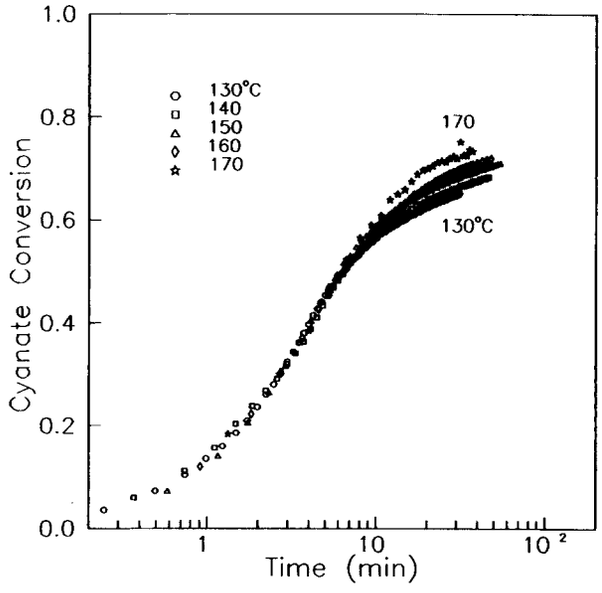

Figure 16 Cyanate conversion at various temperatures vs. equivalent cure time at 170°C

diffusion coefficient vs. cure time. As the resin cures, the diffusivity decreases rapidly. The normalized diffusion coefficient decreases by 3 or 4 orders of magnitude before the resin gels, and approximately 5 orders of magnitude by the end of the cure.

The dependence of the normalized diffusion coefficient on the cyanate conversion is shown in *Figure 15*. The diffusion coefficient decreases slowly at low conversions and quite rapidly at high conversions. The cure dependence of the diffusion coefficient is expected to be related to the structural evolution of the resin system. In addition, at a low conversion, the normalized diffusion coefficient is virtually independent of temperature, while, at a high conversion, the normalized diffusion coefficient is smaller at a low temperature than that at a high temperature. This may be explained by the fact that the diffusion coefficient is a transport property and is dependent on the free volume of the resin. For samples with the same degree of conversion, the difference between the cure temperature and T_g is smaller at a low temperature than at a high temperature. The same is also true for the free volume. Because, at high conversions, T_g approaches the cure temperature, the diffusion coefficient becomes increasingly temperature dependent.

In order to model the reaction kinetics of the cyanate resin, the i.r. data at temperatures lower than 170°C were first horizontally shifted along the time axis to form a single curve overlapping the 170°C curve over the range of conversion between 0 and 40%. This means that, for each cure temperature, the time series of the i.r. data was multiplied by a constant and the constant was then adjusted in value to obtain the best overlay. *Figure 16* shows the results. Below 40% conversion, the data points for all the temperatures form a single curve while, above 40%, the curve starts to diverge and the cyanate conversion is higher at a high temperature than at a low temperature. Consequently, above 40% conversion, the cure kinetics becomes increasingly diffusion-limited but, below 40% conversion, the effect of diffusion on

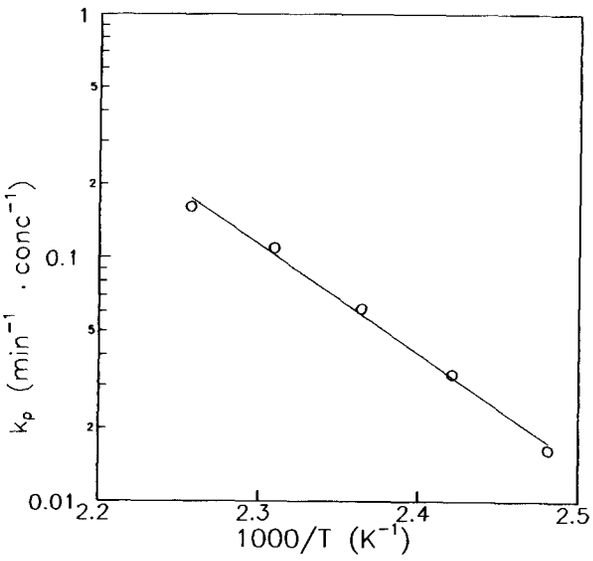

Figure 17 Arrhenius plot of k_p

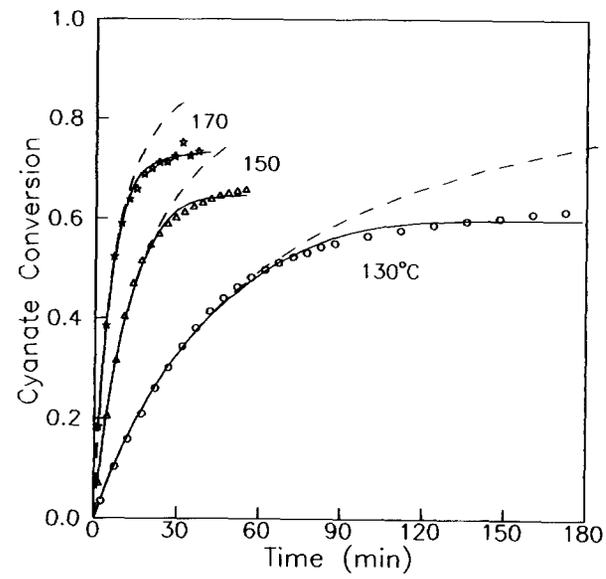

Figure 18 Cure kinetics at various temperatures. . . . . , i.r. data; – – –, second-order rate law, equation (9); ———, diffusion-controlled kinetic model, equation (11)

the kinetics is not evident and the reactions are kinetically controlled. As mentioned earlier, the autocatalytic mechanism is insignificant for the current resin system. The i.r. data below 40% conversion were then used to evaluate the rate constant of the second-order rate law

$$\frac{d\alpha}{dt} = k_p(1-\alpha)^2 \tag{9}$$

where k_p is the rate constant of the second-order kinetics. This rate equation adequately describes the low conversion data (see below). *Figure 17* is the Arrhenius plot for rate constant k_p. The activation energy and the frequency factor were found to be 85.7 kJ mol^{-1} and 2.23×10^9 min^{-1} conc^{-1}, respectively.

The diffusion-controlled cure kinetics of epoxy resins has been analysed using the Rabinowitch model in a number of studies[15,19–21]. The Rabinowitch model was developed for small molecule reactions and is given by

$$\frac{1}{k} = \frac{1}{k_c} + \frac{1}{k_{d0}D} \tag{10}$$

where k is the apparent rate constant which includes the effect of diffusional limitations, k_c is the intrinsic rate constant, and k_{d0} is another constant. By substituting k_p with k and k_c with k_p, equation (9) becomes

$$\frac{d\alpha}{dt} = \frac{k_p k'_{d0}\dfrac{D}{D_{\alpha=0.25}}}{k_p + k'_{d0}\dfrac{D}{D_{\alpha=0.25}}}(1-\alpha)^2 \tag{11}$$

where k'_{d0} $(= k_{d0}D_{\alpha=0.25})$ is a constant. This is the diffusion-controlled kinetic model for the cyanate resin.

With the normalized diffusion coefficient in *Figure 14* and the rate constant k_p in *Figure 17*, equation (11) was solved numerically and was fitted to the experimental i.r. data. *Figure 18* illustrates the modelling results. The prediction of the second-order rate law is in agreement with the experimental data at relatively low conversions. At higher conversions, the mobility of the species are so low that the rate of reaction is significantly reduced and the predicted conversions are higher than the experimental values. The diffusion-controlled model, however, adequately fits the i.r. data over the entire period of cure studied. By altering the apparent rate constant using the diffusion coefficient, this model successfully predicts the deceleration of reactions due to the diffusional limitations. The success of the modelling approach demonstrates that both the Rabinowitch model and the normalized diffusion coefficient obtained are useful in the analysis of the curing kinetics of cyanate resins. The diffusion-controlled model is also expected to find applications in the optimization of the curing processes and in the investigation of other diffusion-related phenomena, such as the effect of diffusion on the gelation of cyanate resins.

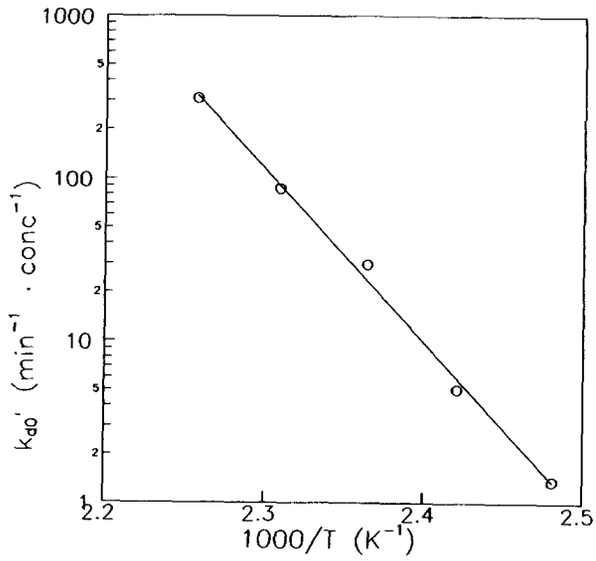

Figure 19 Arrhenius plot of k'_{d0}

Figure 19 is the Arrhenius plot of k'_{d0}. Log k'_{d0} appears to be linearly dependent on $1/T$ over the range of temperatures studied. The activation energy and the frequency factor are 203 kJ mol^{-1} and 2.90×10^{26} min^{-1} conc^{-1}, respectively.

CONCLUSIONS

Because of the absence of strong dipoles in the system, the cyanate resin exhibits weak dipole relaxations. It is difficult to extract dipole relaxation time from the flat loss peaks. While the s.e.c.-measured molecular size distribution agrees with the mean-field prediction at low conversions, the two deviate from each other at relatively high conversions – the experimental weight fractions of short chains are larger than predicted and those of long chains are smaller than predicted, indicating significant diffusional effect. There is, however, no evidence of cure temperature-dependence of the size distribution.

The cure-dependent diffusion coefficient was estimated using equation (1) for the pre-gel stage and equation (3) for the post-gel stage, which decreases approximately 5 orders of magnitude by the end of the isothermal cure.

A diffusion-controlled kinetic model was formulated based on the Rabinowitch model. The prediction of the second-order rate law (the intrinsic kinetic model) is in agreement with the experimental conversion profiles only at relatively low conversions whereas the diffusion-controlled model is good over the range of cure studied. The present work forms the framework for the analysis of the diffusion-controlled kinetics of cyanate resins.

ACKNOWLEDGEMENTS

The authors would like to thank G. P. Kohut and J. T. Gotro of IBM for conducting the dynamic mechanical experiments. The highly purified cyanate resin was provided by HiTek Polymers (currently, a subsidiary of Ciba Geigy).

REFERENCES

1 Owusu, A. O., Martin, G. C. and Gotro, J. T. *Polym. Eng. Sci.* 1991, **31**, 1604
2 Owusu, A. O., Martin, G. C. and Gotro, J. T. *Polym. Eng. Sci.* 1992, **32**, 535
3 Gupta, A. M. and Macosko, C. W. *J. Polym. Sci., Polym. Phys. Edn.* 1990, **28**, 2585
4 Simon, S. L. and Gillham, J. K. *J. Appl. Polym. Sci.* 1993, **47**, 461
5 Bauer, M., Bauer, J. and Jahring, S. *Proc. ACS Div. Polym. Mater. Sci. Eng.* 1992, **66**, 455
6 Shimp, D. A. and Ising, S. J. *Proc. ACS Div. Polym. Mater. Sci. Eng.* 1992, **66**, 504
7 Grigat, E. and Putter, R. *Angew. Chem. Int. Ed.* 1967, **6**, 206
8 Bauer, M., Bauer, J. and Kuhn, G. *Acta Polym.* 1986, **37**, 715
9 Owusu, A. O., PhD Dissertation, Syracuse University, Syracuse, NY, 1992
10 Shimp, D. A. *Proc. ACS Div. Polym. Mater. Sci. Eng.* 1986, **54**, 107
11 Fyfe, C. A., Niu, J., Burlinson, N. E. and Reidsema, C. *Macromolecules* 1992, **25**, 6289
12 Deng, Y. and Martin, G. C. *Macromolecules* 1994, **27**, 5141
13 Deng, Y. PhD Dissertation, Syracuse University, Syracuse, NY, 1994
14 Rabinowitch, E. *Trans. Faraday Soc.* 1937, **33**, 1245
15 Deng, Y. and Martin, G. C. *Macromolecules* 1994, **27**, 5147
16 Deng, Y. and Martin, G. C. *J. Polym. Sci., Polym. Phys. Edn.* 1994, **32**, 2115
17 Day, D. R. *Polym. Eng. Sci.* 1986, **26**, 362
18 Flory, P. J. *J. Am. Chem. Soc.* 1941, **64**, 3091
19 Huguenin, F. G. A. E. and Klein, M. T. *Ind. Eng. Chem., Prod. Res. Dev.* 1985, **25**, 166
20 Havlíček, I. and Dušek, K. in 'Crosslinked Epoxies' (Eds B. Sedláček and J. Kahovec), Walter de Gruyter, Berlin, 1987
21 Rohr, D. F. and Klein, M. T. *Ind. Eng. Chem. Res.* 1990, **29**, 1210